Numerical study of salt fingers dynamics : effects of the density inversion

OUZANI Riadh[a] , KHELLADI Sofiane[b]

[a] LESEI Laboratory, Mechanical Engineering Department, University of Batna 2, Algeria.

[b] Arts et Metiers Institute of Technology, CNAM, LIFSE, HESAM University, F-75013 Paris, France.

Abstract

In the present study, numerical simulations have been employed to understand the effect of the density inversion on the finger structures dynamics and mixing process. A numerical methodology based on the finite volume method with high accuracy schemes were employed to solve the two-dimensional Navier-Stokes equations for high buoyancy ratio ($R_\rho = 6$) and moderate thermal Rayleigh number ($Ra_T = 7\times10^6$). The density is assumed to depend quadratically on the temperature and linearly on the salinity. Three cases of nonlinear parameters were considered : linear case $\varepsilon = 0$, weak nonlinear case $\varepsilon = 1$ and highly nonlinear case $\varepsilon = 3$.

A qualitative and quantitative description of the fingers dynamics emphasizing the mixing properties has been performed. It was found that the density inversion affect significantly the flow pattern, and its motions become asymmetric with respect to the mid-height of the computational domain as nonlinear parameter increase. In the nonlinear cases, the sinking fingers evolve quickly and dramatically increasing, owing to the enhancement of the buoyancy force acting them. The mixing properties were inspected by using the probability density function of the salinity PDF(S*). The results illustrate that the density inversion acts a significant role in the mixing

process. It was shown that the increase in the nonlinear parameter enhances the dynamic of mixing in the lower layer of the system.

Keywords: Double-diffusive convection; Salt finger; Density inversion; Instabilities; Probability density function.

1. Introduction

Fingering convection is a significant topic in research due to its ubiquitous in several natural situations such as oceans [1], lakes [2], and stellar radiative regions [3], as well as in many procedures engineering applications, such as solar ponds [4], storage [5], crystal growth and magma chambers [6], semiconductor [7], geothermal energy [8], and chemical processes [9].

In quiescent aquatic and marine environments, double-diffusive convection can be generated when there is an overall statically stable density gradient, but a slower diffusing component overlies a faster diffusing one. In the oceanography double-diffusion instability can generate when warm salty water overlaying colder fresh water due to the difference in the molecular diffusivities between them [10]. This instability leads to the formation of an alternative sinking and rising of narrow or wide vertical cellular structures, called double-diffusive salt fingers, which can be considered as an important process in the transport of salt and heat [10-11].

During past years, considerable efforts theoretically [12-14], numerically [15-17] and experimentally [18-20], have been conducted to investigate fingering convection in a stagnant ambient. Stern [8] investigated the conditions under which salt finger structures can be occurred by using instability analysis. He reported that salt fingers structures could exist for buoyancy ratio values (expressed as : $R_\rho = \beta_T \Delta T / \beta_S \Delta S$) ranging between from $1 < R_\rho < \tau^{-3/2}$, where $\tau = k_S / k_T$ is the ratio of the diffusivities of the faster diffusing component (originally heat) to the slower diffusing component

(originally salt). This upper limit on the formation of salt fingers was confirmed experimentally by Huppert and Manins [20].

The survey of literature displays that many investigators have focused only on the buoyancy ratio as a key parameter to determine the behavior of the finger characteristics. However, Taylorand Veronis [18], Shen and Veronis [21] revealed that Rayleigh number as independent parameter plays a significant role on the flux ratio produced in the system. Later, Sreenivas et al. [22] demonstrated that the reason for the huge difference in the flux ratio reported by different investigators from laboratory experiments was mainly due to the difference in the thermal Rayleigh number. They also reported that vertical velocity is inversely proportional to the buoyancy ratio and proportional to the Rayleigh number. Furthermore, Singh and Srinivasan [23] demonstrated that a finger characteristic are strongly affected by Rayleigh numbers even if buoyancy ratio remains constant. They revealed that at high Rayleigh numbers the formation of large-scale shearing convection affected the finger growth. The same results are found by Ouzani et al. [24-25] showed that the strong horizontal convection chop off the finger tips, reducing and limiting the finger growth to a value probably even smaller than the initial finger length.

Despite considerable progress in the field of double diffusion fingering convection researchs, up to now, this field is still rich with unresolved problems. In the literature, most analytical and numerical simulations studies of double-diffusive fingering convection dealing with Boussinesq fluid are based on linear density-temperature equation of state as model (e.g. Stern [8], Schmitt [26], Kunze [12] Piacsek and Toomre [27], Ozgokmen et al. [16]). One common aspect of these studies lies in the symmetric evolution of the salt fingers. However, a major anomaly occurs near 4°C (e.g., ice-covered lakes) where the density of water can be varied

non-linearly with the temperature and can be presented a density maximum induced by change in the thermal expansion coefficient sign in the corresponding temperature range (above their freezing temperature), [28], [29]. In this work, we consider a non-linear Boussinesq approach employed by Özgökmen and Esenkov [30] which is quadratic with temperature. In stratifying aquatic systems above their freezing temperature, this non-linear approach may modify the finger structures and their evolution. Indeed, the salt fingers convection becomes more complex where the convective structures evolve asymmetry as has been reported in the laboratory experiments by McDougall and Schmitt [31], [32]. In the same context, several researches [33], [34], [35], have been numerically investigated the effect of the nonlinear equation of state, which is quadratic with temperature, on the Rayleigh-Bénard convection within the pure water around its density maximum at 4°C. They also reported that this special property dramatically alters the nature of convective flows pattern and which leads to breaking the vertical symmetry of the system.

It is well known that cold aquatic environments in which the temperature is below 5°C cover ~70% of the Earth's biosphere and include principally the oceans, and polar regions. These aquatic environmental data prompts us to shed light on fingering convection under these particular conditions whose temperatures are even at subzero. The purpose of this research work is therefore to study the effect of the density inversion induced by the nonlinearity of the equation of state on the finger structures' dynamics and their interactions. We also focus on the diagnostic of the mixing characteristics using the probability density function of salinity.

More recently, Yang and al.[36] have been conducted a computational study of two dimensional and three dimensional direct numerical simulations to analyze the double-diffusive salt finger. They have been indecated strong similarities between

tow and three dimensional results. The same conclusion has been reported by Shen [37] and Kamakura and Ozoe [38]. These studies promote our choice of the two dimensional model used in the current study applied of such systems, see also [39]. Furthermore, it is important to mention that the Reynolds numbers correspond the salt-finger motion are very low (less than 10), which means that the three dimensional turbulent convection is neglected and do not have a dominant effect unlike to the turbulent case [40].

This paper is structured as follows: In **section 2**, we will introduce the physical problem, governing equations, and numerical methods. Next, we will present the simulation results and will discuss the effect of the nonlinearity in the equation of state on the salt-finger convection and mixing properties in **section 3**. Finally, we will give the main conclusions in **section 4**.

2. Mathematical model and numerical method

As shown in figure 1, the model configuration dealt with consists of a rectangular reservoir filled with two different fluids, whose hot and salty fluid lies over a cold and fresh fluid. This initial condition, lead to the formation of an alternative rising and sinking convective structures in the computational domain. The system is subject to the gravity action-oriented in a negative z -direction.

Throughout the current study, the thermophysical properties of the both salty and fresh fluid are kept constant except for the density variation, whose we adopt the Boussinesq assumption to describe the density of the fluid as follows [31]:

$$\rho(T,S) = \rho_0 \left[1 - \beta_{T_1}(T - T_0) + \beta_S (S - S_0) - \beta_{T_2}(T - T_0)^2 \right] \quad (1)$$

Where T_0, S_0 and ρ_0 are the reference temperature, salinity and density, respectively. The variation of the density induced by the temperature variation is

defined by linear and nonlinear terms with corresponding expansion coefficients β_{T_1} and β_{T_2}, while β_S is the linear contraction coefficient for salinity.

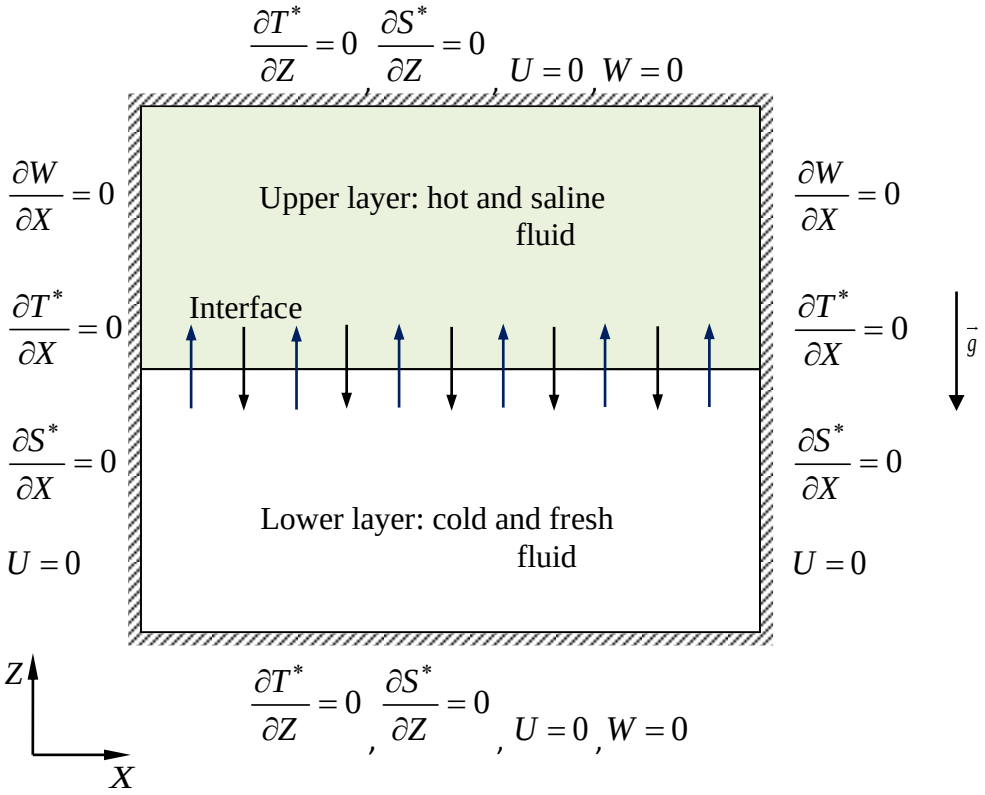

Figure1. Physical model for double diffusive fingering convection showing initial and boundary conditions.

To facilitate the analysis of the effect of this nonlinear density relationship on the salt finger system, we introduce the nonlinear parameter which expressed as : $\varepsilon = 2\beta_{T_2}\Delta T / \beta_{T_1}$.

The two-dimensional governing equations for the double-diffusive system are given as follows [22], [25],[41]:

$$\frac{\partial u}{\partial x}+\frac{\partial w}{\partial z}=0 \tag{2}$$

$$\frac{\partial u}{\partial t}+u\frac{\partial u}{\partial x}+w\frac{\partial u}{\partial z}=-\frac{1}{\rho_0}\frac{\partial p}{\partial x}+\nu\left(\frac{\partial^2 u}{\partial x^2}+\frac{\partial^2 u}{\partial z^2}\right) \tag{3}$$

$$\frac{\partial w}{\partial t}+u\frac{\partial w}{\partial x}+w\frac{\partial w}{\partial z}=-\frac{1}{\rho_0}\frac{\partial p}{\partial z}+\nu\left(\frac{\partial^2 w}{\partial x^2}+\frac{\partial^2 w}{\partial z^2}\right)-\left(1-\beta_{T_1}(T-T_0)+\beta_S(S-S_0)-\beta_{T_2}(T-T_0)^2\right)g \tag{4}$$

$$\frac{\partial T}{\partial t}+u\frac{\partial T}{\partial x}+w\frac{\partial T}{\partial z}=k_T(\frac{\partial^2 T}{\partial x^2}+\frac{\partial^2 T}{\partial z^2}) \quad (5)$$

$$\frac{\partial S}{\partial t}+u\frac{\partial S}{\partial x}+w\frac{\partial S}{\partial z}=k_S(\frac{\partial^2 S}{\partial x^2}+\frac{\partial^2 S}{\partial z^2}) \quad (6)$$

Where u, w, p, T and S are the velocity components, pressure and temperature and concentration of fluid, respectively. ν. k_T and k_S are the kinematic viscosity, thermal and concentration diffusivity, respectively.

	thermal diffusivity	salinity diffusivity	thermal expansion coefficient	salinity expansion coefficient	kinematic viscosity	domain height	aspect ratio
Unity	k_T $\left[m^2 s^{-1}\right]$	k_S $\left[m^2 s^{-1}\right]$	β_{T_1} $\left[{}^0C^{-1}\right]$	β_S $\left[s^{-1}\right]$	ν $\left[m^2 s^{-1}\right]$	H $[m]$	Ar
Values	1.4×10^{-7}	1.4×10^{-9}	2×10^{-4}	8×10^{-4}	1.0×10^{-6}	0.15	0.5

Table 1- Thermophysical properties of the double diffusive system.

The corresponding dimensionless governing equations system are given as follows[25]:

$$\frac{\partial U}{\partial X}+\frac{\partial W}{\partial Z}=0 \quad (7)$$

$$\frac{\partial U}{\partial t^*}+U\frac{\partial U}{\partial X}+W\frac{\partial U}{\partial Z}=-\frac{\partial P}{\partial X}+\Pr(\frac{\partial^2 U}{\partial X^2}+\frac{\partial^2 U}{\partial Z^2}) \quad (8)$$

$$\frac{\partial W}{\partial t^*}+U\frac{\partial W}{\partial X}+W\frac{\partial W}{\partial Z}=-\frac{\partial P}{\partial Z}+\Pr(\frac{\partial^2 W}{\partial X^2}+\frac{\partial^2 W}{\partial Z^2})+\Pr(Ra_T\ T^*(1+\frac{\varepsilon}{2}T^*)-Ra_S S^*) \quad (9)$$

$$\frac{\partial T^*}{\partial t^*}+U\frac{\partial T^*}{\partial x}+W\frac{\partial T^*}{\partial Z}=\left(\frac{\partial^2 T^*}{\partial X^2}+\frac{\partial^2 T^*}{\partial Z^2}\right) \quad (10)$$

$$\frac{\partial S^*}{\partial t^*}+U\frac{\partial S^*}{\partial X}+W\frac{\partial S^*}{\partial Z}=\frac{\Pr}{Sc}\left(\frac{\partial^2 S^*}{\partial X^2}+\frac{\partial^2 S^*}{\partial Z^2}\right) \quad (11)$$

$$X=\frac{x}{H},\ Z=\frac{z}{H},\ t^*=\frac{tk_T}{H^2},\ U=\frac{uH}{k_T},\ W=\frac{wH}{k_T},\ P=\frac{pH^2}{k_T^2\rho_0},\ T^*=\frac{T-T_{bottom}}{\Delta T},\ S^*=\frac{S-S_{bottom}}{\Delta S}$$

Where X and Z are the cartesian coordinates in the horizontal and vertical directions, respectively , t^* is the time, U and W the velocity components, P is the pressure, T^* is the temperature and S is the salinity. $\Delta T = T_{Top} - T_{Bottom}$, and $\Delta S = S_{Top} - S_{Bottom}$ are the temperature and the salinity differences between the top and bottom layers.

The dimensionless parameters are : Prandtl number $\Pr = \frac{\nu}{k_T}$, Schmidt number $Sc = \frac{\nu}{k_S}$, thermal Rayleigh number $Ra_T = \frac{g\beta_{T_1}\Delta T H^3}{\nu k_T}$, and salinity Rayleigh number $Ra_S = \frac{g\beta_S \Delta S H^3}{\nu k_S}$.

The boundary conditions in the dimensionless form are given as follows [22], [23]:

$$U = 0, \frac{\partial W}{\partial X} = 0, \frac{\partial T^*}{\partial X} = 0, \frac{\partial S^*}{\partial X} = 0 \text{ at } X = 0, 0 \le Z \le H \quad \text{(12-a)}$$

$$U = 0, \frac{\partial W}{\partial X} = 0, \frac{\partial T^*}{\partial X} = 0, \frac{\partial S^*}{\partial X} = 0 \text{ at } X = B, 0 \le Z \le H \quad \text{(12-b)}$$

$$U = W = 0, \frac{\partial T^*}{\partial Z} = 0, \frac{\partial S^*}{\partial Z} = 0 \text{ at } Z = 0, 0 \le X \le B \quad \text{(12-c)}$$

$$U = W = 0, \frac{\partial T^*}{\partial Z} = 0, \frac{\partial S^*}{\partial Z} = 0 \text{ at } Z = H, 0 \le X \le B \quad \text{(12-d)}$$

For the initial conditions ($t^* = 0$), the fluid is considered stationary and a step profile across a horizontal interface at mid-depth ($Z = 0.5$) is imposed for both temperature and salinity [53]:

$$(U, W) = (0, 0)$$
$$T^*(X, t^* = 0) = \begin{cases} \Delta T^* & \text{for } Z \ge 0 \\ 0 & \text{for } Z < 0 \end{cases} \quad \text{(12-e)}$$

$$S(X,t^*=0)=\begin{cases}\Delta S^* & \text{for} \quad Z\geq 0\\ 0 & \text{for} \quad Z<0\end{cases}$$

2.1. Computational procedure

In this study, the numerical methodology that was employed to solve the dimensionless Navier–Stokes equations (8-11) is described as the following:

- **Approximation of the convective and the diffusive terms**

The tow-dimensional diffusion-convection equations (8-11) are rewritten as:

$$\frac{\partial f}{\partial t^*}=L(f) \tag{13}$$

$$L(f)=A\left(\frac{\partial^2 f}{\partial X^2}+\frac{\partial^2 f}{\partial Z^2}\right)-U\frac{\partial f}{\partial X}-W\frac{\partial f}{\partial Z}+D=\phi_{diff_{i,j}^n}+\phi_{conv_{i,j}^n}+D \tag{14}$$

where f represents U, W, T^*, S^* and the term source D.

The discretization scheme for the second partial derivatives $\frac{\partial^2 f}{\partial X^2}$, $\frac{\partial^2 f}{\partial Z^2}$ can be obtained by using employing central differencing with fourth-order accuracy.

The discretization scheme for the first partial derivatives $\frac{\partial f}{\partial X}$, $\frac{\partial f}{\partial Z}$ can be obtained by using the fifth-order WENO scheme [42], [43] as follow:

We calculate the smoothness indicators $IS_i, i=0,1,2$.

The IS_i^+ are given by:

$$IS_0^+=\frac{13}{12}(f_{j-2}^+-2f_{j-1}^++f_j^+)^2+\frac{1}{4}(f_{j-2}^+-4f_{j-1}^++3f_j^+)^2, \tag{15}$$

$$IS_1^+=\frac{13}{12}(f_{j-1}^+-2f_j^++f_{j+1}^+)^2+\frac{1}{4}(f_{j-1}^+-f_{j+1}^+)^2, \tag{16}$$

$$IS_2^+=\frac{13}{12}(f_j^+-2f_{j+1}^++f_{j+2}^+)^2+\frac{1}{4}(3f_j^+-4f_{j+1}^++f_{j+2}^+)^2, \tag{17}$$

And the IS_i^- are given by:

$$IS_0^- = \frac{13}{12}(f_{j+1}^- - 2f_{j+2}^- + f_{j+3}^-)^2 + \frac{1}{4}(3f_{j+1}^- - 4f_{j+2}^- + f_{j+3}^-)^2, \tag{18}$$

$$IS_1^- = \frac{13}{12}(f_j^- - 2f_{j+1}^- + f_{j+2}^-)^2 + \frac{1}{4}(f_j^- - f_{j+2}^-)^2, \tag{19}$$

$$IS_2^- = \frac{13}{12}(f_{j-1}^- - 2f_j^- + f_{j+1}^-)^2 + \frac{1}{4}(f_{j-1}^- - 4f_j^- + 3f_{j+1}^-)^2, \tag{20}$$

we compute the nonlinear stencil weights :

$$\alpha_i^{\pm} = \frac{d_i}{(\varepsilon + IS_i)^2}, i = 0,1,2$$

Here we choose $\varepsilon = 10^{-6}$ to avoid the denominator to become zero. The linear weights are given by:

$$d_0 = \frac{1}{10},\ d_1 = \frac{6}{10},\ d_2 = \frac{3}{10}$$

and

$$\alpha_0^{\pm} = \frac{1}{10}\left(\frac{1}{\varepsilon + IS_0^{\pm}}\right)^2, \quad \alpha_1^{\pm} = \frac{6}{10}\left(\frac{1}{\varepsilon + IS_1^{\pm}}\right)^2, \quad \alpha_2^{\pm} = \frac{3}{10}\left(\frac{1}{\varepsilon + IS_2^{\pm}}\right)^2 \tag{21}$$

In order to get a convex combination of ENO stencils, the WENO stencil weights are normalized to give:

$$w_0^{\pm} = \frac{\alpha_0^{\pm}}{\alpha_0^{\pm} + \alpha_1^{\pm} + \alpha_2^{\pm}}, \quad w_1^{\pm} = \frac{\alpha_1^{\pm}}{\alpha_0^{\pm} + \alpha_1^{\pm} + \alpha_2^{\pm}}, \quad w_2^{\pm} = \frac{\alpha_2^{\pm}}{\alpha_0^{\pm} + \alpha_1^{\pm} + \alpha_2^{\pm}} \tag{22}$$

where: $w_j^{\pm} \in (0,1)$, $j = 0,1,2$, and $w_0^{\pm} + w_1^{\pm} + w_2^{\pm} = 1$

Finally, the numerical fluxes are defined as:

$$\begin{aligned}\hat{f}_{j+\frac{1}{2}}^{+} &= w_0^{+}\left(\frac{2}{6}f_{j-2}^{+} - \frac{7}{6}f_{j-1}^{+} + \frac{11}{6}f_j^{+}\right) + w_1^{+}\left(-\frac{1}{6}f_{j-1}^{+} + \frac{5}{6}f_j^{+} + \frac{2}{6}f_{j+1}^{+}\right) \\ &+ w_2^{+}\left(\frac{2}{6}f_j^{+} + \frac{5}{6}f_{j+1}^{+} - \frac{1}{6}f_{j+2}^{+}\right)\end{aligned} \tag{23}$$

and

$$\hat{f}^{-}_{j+\frac{1}{2}} = w_2^{-}\left(-\frac{1}{6} f^{-}_{j-1} + \frac{5}{6} f^{-}_{j} + \frac{2}{6} f^{-}_{j+1}\right) + w_1^{-}\left(\frac{2}{6} f^{-}_{j} + \frac{5}{6} f^{-}_{j+1} - \frac{1}{6} f^{-}_{j+2}\right) + w_0^{-}\left(\frac{11}{6} f^{-}_{j+1} - \frac{7}{6} f^{-}_{j+2} + \frac{2}{6} f^{-}_{j+3}\right) \tag{24}$$

$$\phi_{conv^{n}_{i,j}} = -\frac{1}{\Delta x}\left[\left(\hat{f}^{+}_{j+\frac{1}{2}} - \hat{f}^{+}_{j-\frac{1}{2}}\right) + \left(\hat{f}^{-}_{j+\frac{1}{2}} - \hat{f}^{-}_{j-\frac{1}{2}}\right)\right] \tag{25}$$

- **Approximation of time**

For the time approximation of equation (13), we employed the third-order accurate TVD Runge-Kutta scheme to advance in time:

$$f^{(1)} = \gamma_1 f^{n} + \gamma_1' \Delta t^{*} L(f^{n}) \tag{26}$$

$$f^{(2)} = \gamma_2 f^{n} + \gamma_2'\left[f^{(1)} + \Delta t^{*} L(f^{(1)})\right] \tag{27}$$

$$f^{n+1} = \gamma_3 f^{n} + \gamma_3'\left[f^{(2)} + \Delta t^{*} L(f^{(2)})\right] \tag{28}$$

where: $\gamma_1 = 1$, $\gamma_2 = \frac{3}{4}$, $\gamma_3 = \frac{1}{3}, \gamma_1' = 1$, $\gamma_2' = \frac{1}{4}$, $\gamma_3' = \frac{2}{3}$ and Δt^{*} is the time step. For further details see Gottlieb and Shu [44].

2.2. Numerical validation tests

In order to verify the accuracy and the correctness of the in-house code used in the current study we have considered the work carried out by Nishimura et al. [45] as a reference case which is corresponding to double-diffusive natural convection flow in a vertical rectangular enclosure. Their work is considered as an excellent benchmark which employed extensively by many investigators (see, for instance, [46], [47], [48]) to check the validity and the efficiency of computational codes.

The computational conditions are as follows: the Prandtl number $\mathrm{Pr}=1$; the Lewis number $Le=2$ and the Rayleigh number $Ra=10^5$. The buoyancy ratios values used ($R_\rho=1.3,\ 1.3$ and 1) cover different flow regimes. The same dimensions (aspect ratio $Ar=2$) and grid resolution (31×41) as [45] were performed.

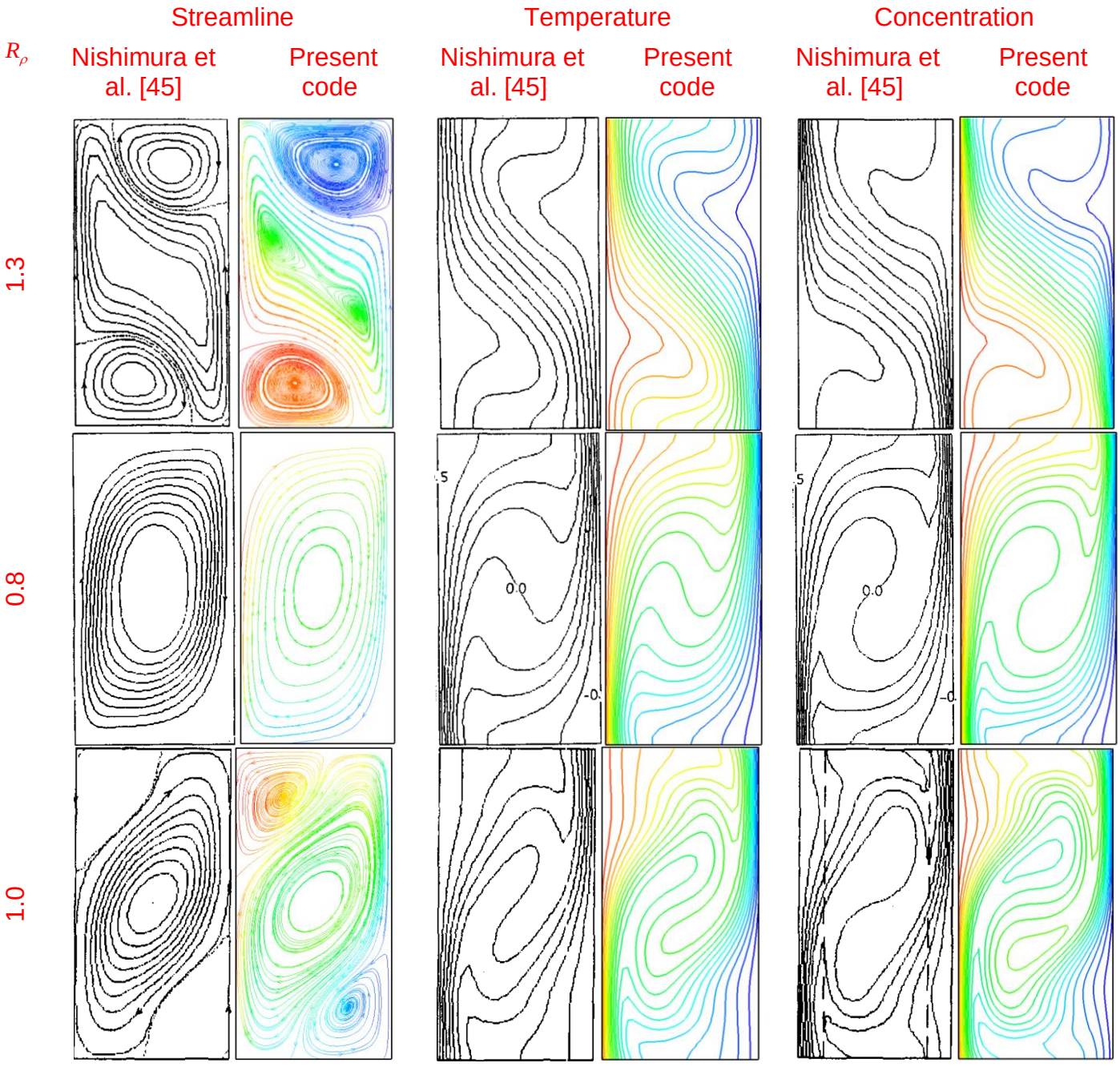

Figure 2. Comparisons between the results from the present code and the numerical results from Nishimura et al. [45].

Figure 2 display a clear comparison between numerical results of (streamline, isotherms and concentration) plots obtained by the present code and those of Nishimura et al. [45]. Three behaviors of the steady flow have been taken in counts corresponding to thermally dominated flow, compositional dominated flow oscillatory flow corresponding to the buoyancy ratios $R_\rho = 1.3$, $R_\rho = 0.8$ and $R_\rho = 1$, respectively. As can be seen, the comparison showing a good concordance with the results reported by Nishimura et al. [45], thus corroborates the capacity and the numerical accuracy of our computational code for simulating the double-diffusive natural convection flow.

The reliability of the computational method to capture accurately the finger structures and their evolution/interaction in time and space was also confirmed by reproducing the results published in the literature, Ref. [25].

3. Results and discussions

In this section we investigate the influence of the density inversion, induced by the nonlinearity of the equation of state, on the development of fingers and their dynamics. To do this, three numerical tests have been reported regarding the nonlinear parameter $\varepsilon = 0$, $\varepsilon = 1$ and $\varepsilon = 3$. The first case 1 ($\varepsilon = 0$) which corresponds to the linear equation of state for comparison. The nonlinear term activates when $\varepsilon > 0$. Indeed, for the second case ($\varepsilon = 1$) the nonlinear term becomes important compared to the linear term for temperature. For the third case ($\varepsilon = 3$) the nonlinear term becomes predominant in the equation of state. The results of our numerical simulations have been performed with 400×300 grids mesh, which selected as an optimal number of nodal points to solve accurately the evolution pattern of finger convection in the enclosure. In the present work, we set the Prandtl and the Schmidt numbers at 7 and 700, respectively, i.e., the Lewis

number $Le = 100$, which are the typical values for seawater system see, e.g., [49], [50]. For all simulations the buoyancy ratio, the thermal Rayleigh number and salinity Rayleigh number were held fixed at $R_\rho = 6$, $Ra_T = 7 \times 10^6$ and $Ra_S = 1.167 \times 10^6$.

3.1. Finger structures dynamics and mixing properties

a) Reference case : linear equation of state

We start by looking at the first case $\varepsilon = 0$, this linear case constitutes a reference that helps us to quantify well the effect of the the nonlinearity of the equation of state on the salt fingers evolution.

Figure 3 (a-f) shows a global glimpse of evolution of salt fingers convection at buoyancy ratio $R_\rho = 6$ from a dynamic point of view.

In the initial phase, we can see that the interface separating the cold and fresh fluid starts to thickness linearly with time due to a purely molecular diffusion. With time the interface separating becomes unstable and begins to take a wavy shape see figure 3 (c). afterwards, structures in the form of mushroom plumes have been developed from this interface. We can clearly distinguish the formation of thirty-six finger columns (eighteen pairs of rising and sinking cells) which corresponds exactly to the number of waves in the interface.

In the inside of each finger, the salt concentration is preserved and maintains the initial value of the layer from which it originates ($S^* = 0$ for the rising fingers and $S^* = 1$ for sinking fingers), with the exception of the fingreing interface where still changed by molecular diffusion process. The fingers structures grow rapidly due to the acceleration of the flow induced by advection motion see the velocity vector (figure 4(a)). Because the mass flux is conserved inside the fingers, we observe a reduction

of fingers width with increasing in its length. Hence, fingers take a vertical wavy form which makes them gravitationally unstable.

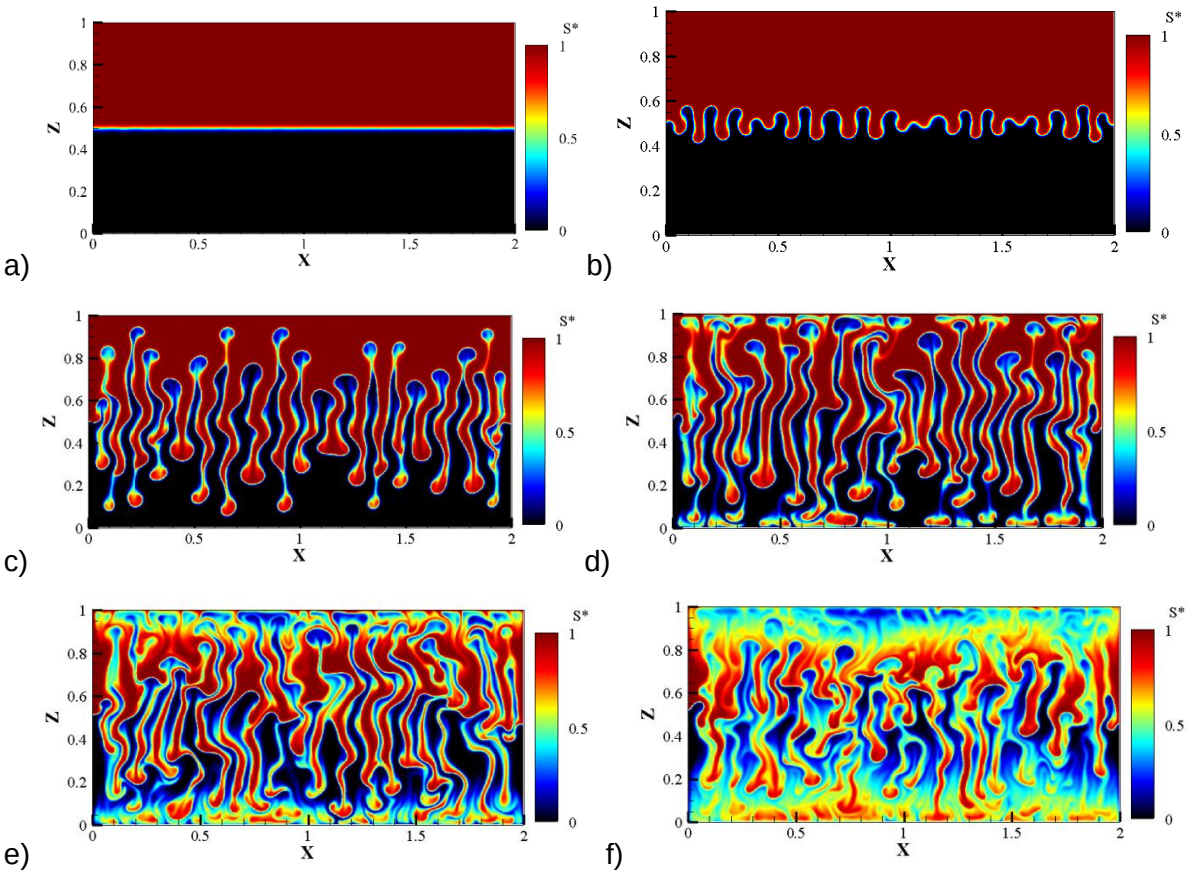

Figure 3. Evolution of salt-fingers at 10 h, 14 h 40 min, 20 h, 23h , 26 h 25 min, 30 h 30 min, 38 h 6 min and 46 h, respectively. In this case $Ra_T = 7.\times 10^6$, $R_\rho = 6$ and $\varepsilon = 0$.

At the end of the each finger we observe an engulfment at the finger tips due to the accumulation of the fluid called blob structures (figure 3 (c)), as found by Taylor and Veronis [51]. As time elapses, these blobs become unstable due to the gravity effect and detached from the finger bodies and become independent cores in the form of vortex dipoles called ‘bulbous’ (figure 4 (b)). These structures have been observed in previous works, by Pringle and Glass [52] and Rehman and Singh [53]. We also notice that when blobs break off from the finger bodies a new blob regenerated and replaced them.

When fingers reach the ends of the domain, we observe the formation of so-called umbrella-shaped structure that spread horizontally and becomes flat allowing to

coalesce together (see figure 3 (d-e)) and this lead to the formation of the upper and lower mixed layers in the same time as shown figure 3 (f). As results, the salt finger structures sandwiched between these mixed layers forming so-called 'salt-finger zone'. In this stage, the system becomes dynamically less active and the vertical salinity flux diminish.

In the final stage, the salt finger structures begin to vanish, as consequence, the mixing activity weaken and the system become dominated by molecular diffusion. The main important conclusion, in this linear case, is the strong symmetry of the flow motions between upper and lower layers about the mid-height of the computational domain, in contrast to the nonlinear cases that will be discussed in the following subsection.

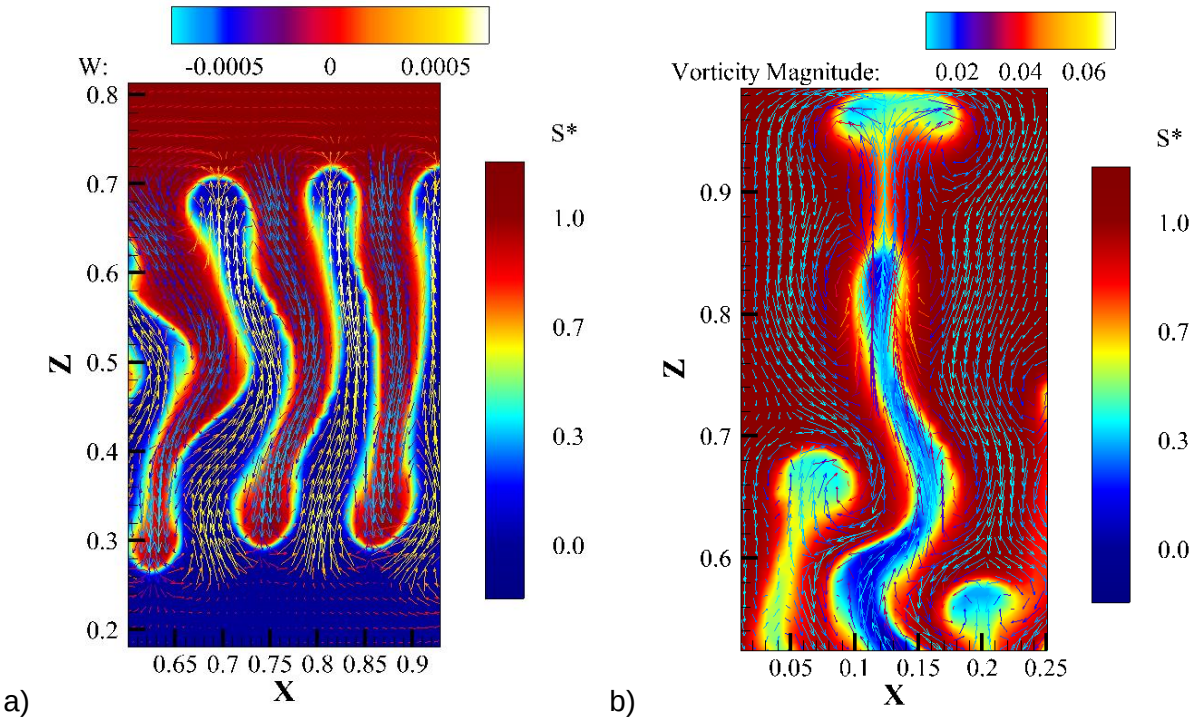

Figure 4. Close-up view of : a) instantaneous contours of salinity field on which the velocity vector is superimposed, b) isolated blob on which the velocity vector (colored by vorticity magnitude) is superimposed to illustrate the dipolar vortex.

The figure 5 (a) show the horizontal averaged profiles of salinity at different times. At t=0, the initial distribution of the salinity takes value $S^* = 0$ for $0 < Z < 0.5$ and $S^* = 1.0$

for $0.5 < Z < 1$ which corresponding to the salinity of the upper and lower layers respectively.

For (t<2h), salt profiles are almost identical to the initial distribution state with a weak change at the mid-height of the computational domain produced by diffusive processes.

As time increases (t > 13 h 15 min), salt profiles begin to spread progressively about the mid-height of the domain forming the so-called 'spread zone'. Indeed, at t = 15 h 50 min, we can see that in the range $Z < 0.35$ and $Z > 0.65$ the values of salt keep their initial values $S^* = 0$ and $S^* = 1$ correspond to the lower and upper layers respectively, whereas, outside these ranges, salt takes values between $0 < S^* < 1$ (this means that salt gradient $S^*_{Top} - S^*_{Bottom} = \Delta S^* \approx 1.0$).

When the time t > 19 h 50 min, the salt gradient becomes $\Delta S^* < 1.0$ which implies that the salt fingers reach the ends of the domain. We notice that with the formation of mixed layers the initial distribution of the salinity disappears completely.

As time increases, mixing efficiency in the salt-finger system increase, and the salinity tends to an asymptotic value $S^* = 0.5$ which makes the salinity distributions uniform in the system (i.e., salt gradient $\Delta S^* \to 0$) and constitutes stable layers at the end (figure 10 (a) at t = 29 h 30 min). It is interesting to note that profiles remain symmetric in this case in time.

Figure 5 (b) depicts the temporal evolution of non-dimensional kinetic energy representing as E_k is given by $E_k = 1/2 < U^2 + W^2 >$, where $< >$ means averaged domain.

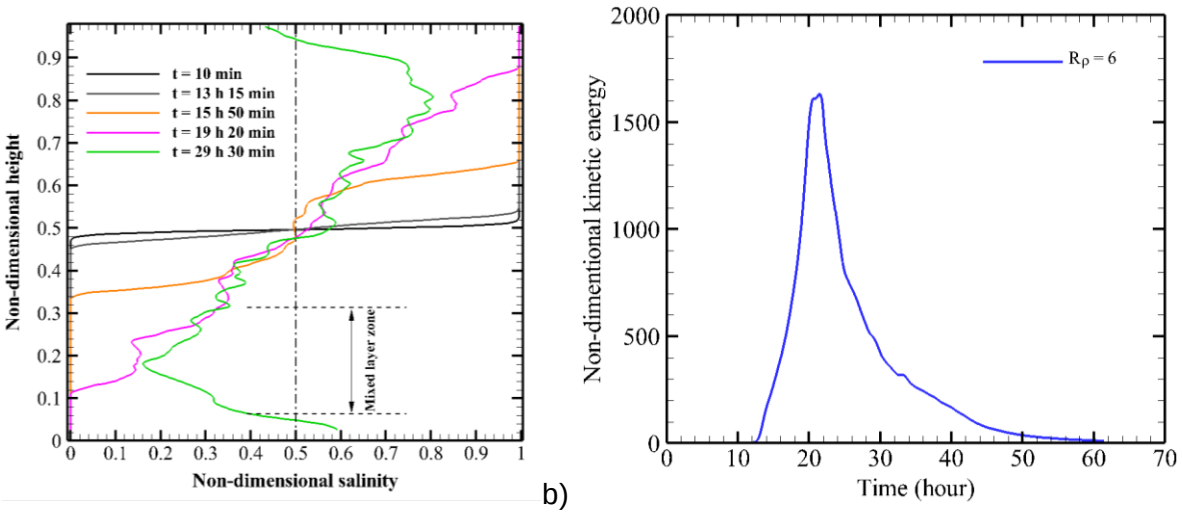

Figure 5. a) Vertical profiles of mean salinity, b) Time evolution of the system kinetic energy. In this case, $Ra_T = 7.\times 10^6$ and $R_\rho = 6$ and $\varepsilon = 0$.

When analyze the evolution of kinetic energy, we can observe three distinct stages. In the first stage, kinetic energy $E_k = 0$ which implies the total energy of the system is initially stored in the form of the potential energy in the salinity interface. In the second stage $13h < t^* \le 25h$, with the development of the finger structures, the potential energy of the system is released and converted into kinetic energy and the kinetic energy quickly reaches its maximum value $E_k = 1650$. In the last stage $t^* > 25h$, the kinetic energy of the system starts to decrease again progressively with time under the effects of the viscosity, and the fingers' motion is damped and disappears completely.

We now discuss the mixing process induced by double convection salt finger, we use the probability density function of the salinity PDF(S*), [54-56]. The PDF(S*) is considered an excellent tool to quantify the evolution of the mixing properties of the system.

Figure 6 illustrates the evolution of probability density functions 'PDFs' in the z-direction at different times. For all simulations, we displace the origin location to the middle of the domain (i.e., the center of the symmetric of the system) in order to

better quantified the contrast in the mixing between upper and lower layers with respect to the nonlinear parameter.

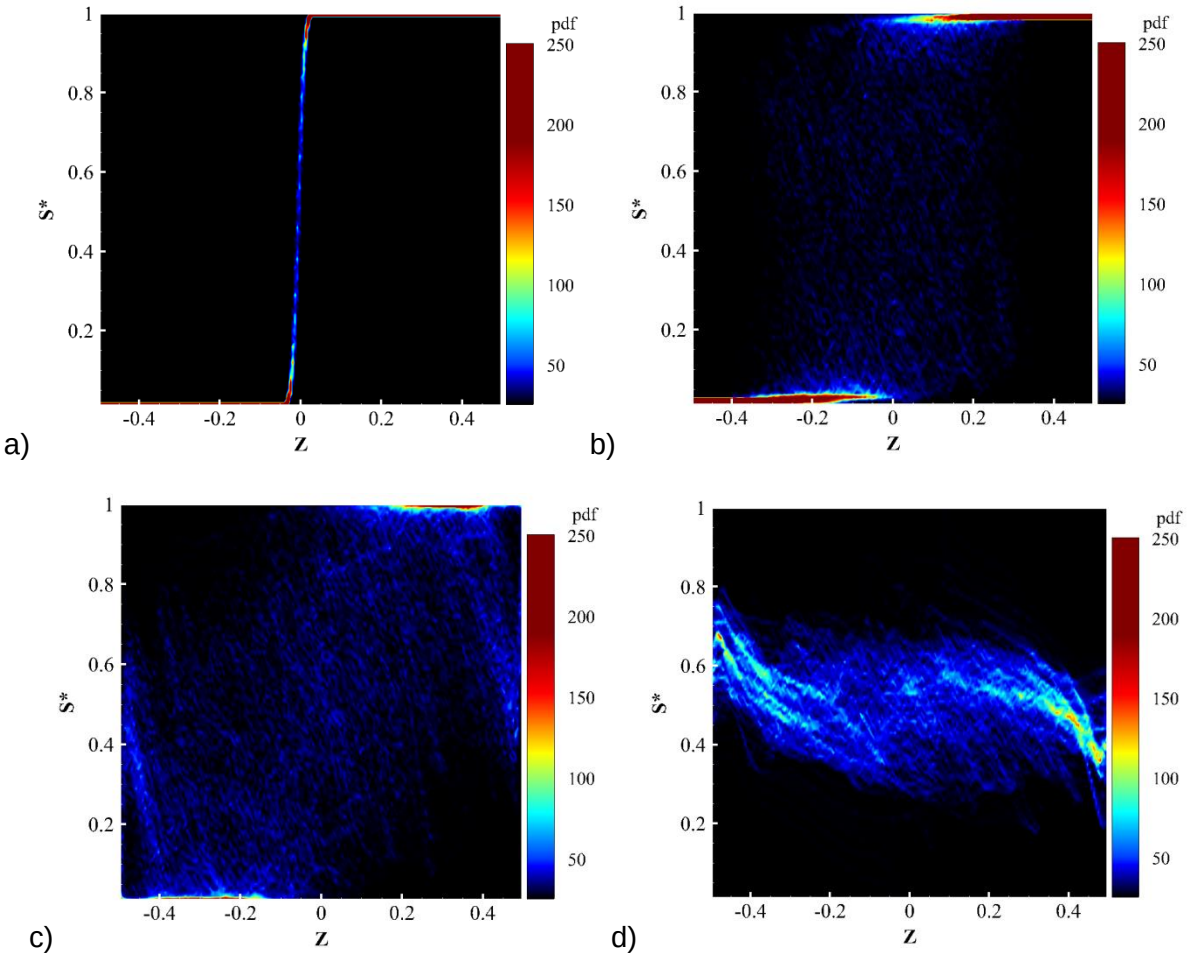

Figure 6. Evolution of the probability density function at moderate thermal Rayleigh number $Ra_T = 7.\times 10^6$ for $R_\rho = 6$ and $\varepsilon = 0$.

The PDF distribution in figure 6 (a) illustrates that there is a very weak mixing activity near the mid-height of the domain $Z = 0$ which is driven by molecular diffusion.

As time passes, PDF shows abroad range of the salinity having weak PDF values take place in the zone limited between $Z = -0.3$ and $Z = 0.3$. This zone known as the "diffusion zone", see figure 6 (b).

It must also be noted that there is a high probability to find pure unmixed salt with salinity values $S^* = 0$ and $S^* = 1$ corresponding to the lower and upper layers, respectively. This can be explained by the fact that finger structures grow

monotonically without interactions. Indeed, large amounts of salt are moved up and down without mixing, as the fluids inside the fingers maintain their initial values (figure 6 (b)).

The diffusion zone continues to extend with time as fingers increased in a monotonous way and encompass the whole domain without interacting dynamically with their neighbors. Consequently, the mixing process in this stage remains controlled by molecular diffusion. It is important to note that the mixing process between the upper and lower layers is symmetric with respect to the mid-domain.

When fingers reach the domain ends, the mixing is enhanced close to the boundaries due to the horizontal spread of the bulbous which merges bulbous with each other and forms so-called mixed layers see figure 6 (c). The PDF indicates that there is no probability to find pure unmixed fluid close to the top and bottom boundaries. Furthermore, the PDF refers that salinity taking values range between $0.4 < S^* < 0.6$, this implies that the mixing appears practically in equal proportion and becomes more homogeneous in these regions (see figure 6 (d)). Conversely, a high probability of pure unmixed salt is detected in the zone spanning in $-0.4 < Z < 0.4$ namely the "finger zone" (see figure 6 (c)). In this region, fingers with pure unmixed liquid remain trapped between the mixed layers because they are less dynamic, hence the mixing intensity is very weak. This finding is well corroborated by figure 3 (f).

As time progresses, the finger zone becomes more dynamic and the probability of finding values of salinity confined between $0.4 < S^* < 0.6$ is clearly visible in the mid-domain proving hence the better mixing of the fluid.

Moreover, in the vicinity of the computational domain ends, we note that convection becomes less intense allowing again the injection of pure salt into the mixed layers

as referred in the PDF distribution. Indeed, the salinity values are ranging $0.6 < S^* < 0.8$ in the upper mixed layer and $0.4 < S^* < 0.2$ in the lower mixed layer.

b) Nonlinear equation of state effect

Turning now to the influence of nonlinearity of the equation of state on the development of fingers, their dynamics and we will also look at mixing properties. In this study two cases of nonlinear parameters have been then considered: weak nonlinear case $\varepsilon = 1$ and highly nonlinear case $\varepsilon = 3$.

The first overview in figure 8 shows clearly that the number of fingers developed in the system is identical to this of the linear case (18 pairs of rising and sinking). However, the qualitative analysis of instantaneous salinity fields reveals a net difference in the rising and sinking fingers dynamics especially at highly nonlinear case, compared to the linear case.

The flow system starts by the stable phase generated from the initial state where no fingers have been detected at the interface (this phase has not been presented in figure 8). This phase is characterized by an increase in the interface thickness under the effect of molecular diffusion in both cases like in the linear one. In the following phase, we observe the appearance of instability at the interface, which leads to its undulation and then the trigger of the wavy fingers structures, see figure 8 (a-d). We note that the onset of instability is delayed unlike the linear. The physical reason for this delay is that the fingering interface becomes stably stratified due to the increase of the nonlinear parameter ε which improved the stabilizing effect of the temperature, see figure 9 (e) and (f). Hence, the effect of the nonlinear parameter prevents the formation of the rising fingers while promoting the sinking finger motion.

In the next phase, for the weakly nonlinear case figure 8 (e), a monotonic increase in the fingers' length is obvious. Therefore, fingers can still grow the whole height of the

computational domain without interacting. As distinct feature of the linear case, rising fingers ascend slowly compared to those sinking, see figure 9 (a). As a consequence, the evolution of rising fingers length is slightly smaller than the sinking.

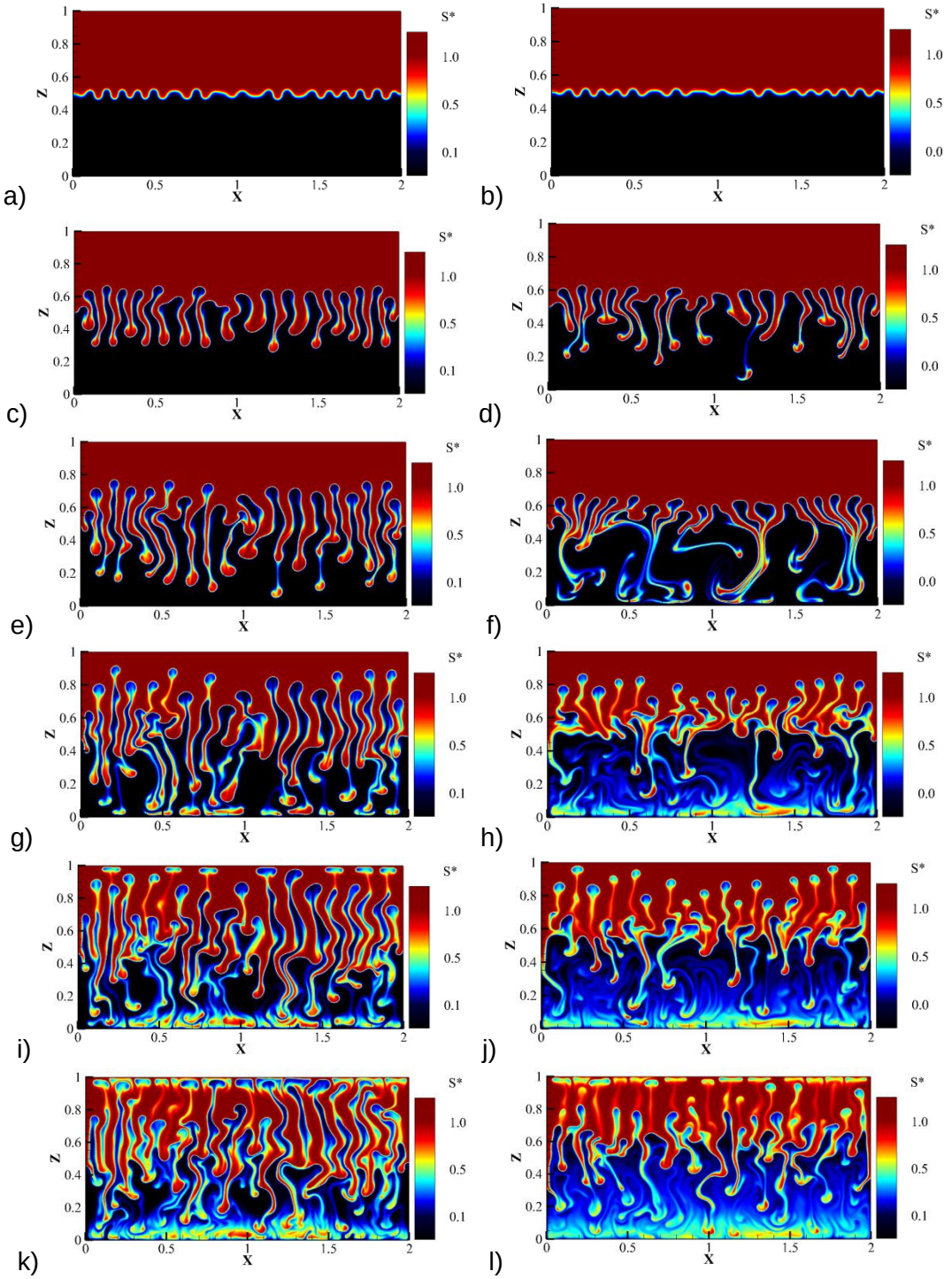

Figure 8. Evolution of salt-fingers at moderate thermal Rayleigh number $Ra_T = 7.\times 10^6$ and $R_\rho = 6$ ($\varepsilon = 1$, left panel), ($\varepsilon = 3$, right panel).

A quantitative comparison of finger lengths indicates that rising fingers occup approximately 45% height of the computational domain compared to the sinking occupying 25% see figure 8 (e). Furthermore, the sinking fingertips are characterized by intense vorticity, high vertical velocity, and kinetic energy as shown in the figures 9 (a), (c) and 10 (a) and 10 (c). Moreover, in figure 8 (g) we clearly see that the sinking fingers reach the end of the field before the rising fingers and hence begin to interact with the boundary resulting the earlier formation of the lower mixed layer contrary to the upper one in the figure 9 (i) and (k).

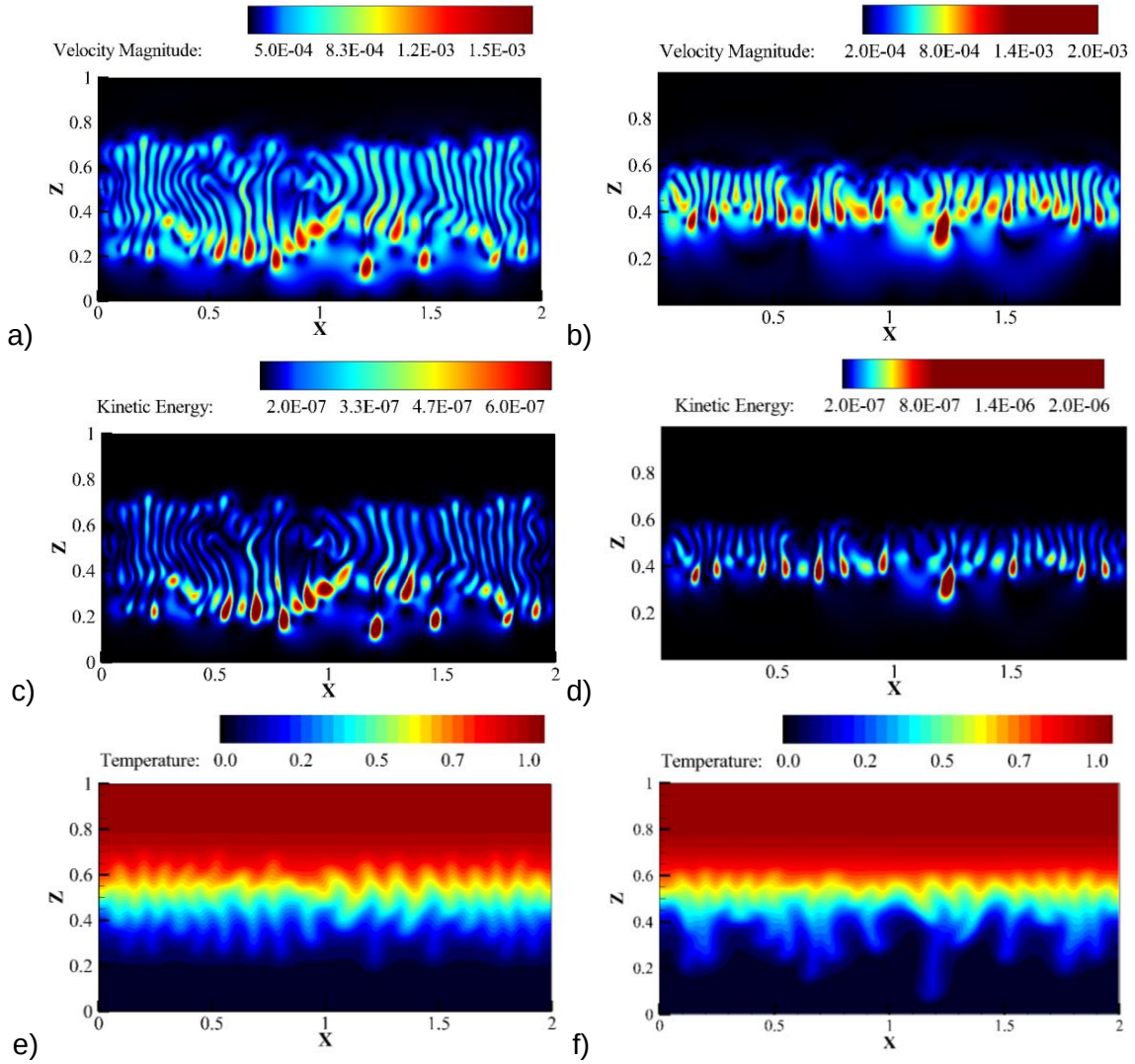

Figure 9. Instantaneous contours of : a-b) velocity , c-d) kinetic energy , e-f) temperature, at moderate thermal Rayleigh number $Ra_T = 7.\times 10^6$ and $R_\rho = 6$: ($\varepsilon = 1$ left panel), ($\varepsilon = 3$,right panel).

For the highly nonlinear case ($\varepsilon = 3$), the evolution of the fingers is qualitatively very different and seems more complicated from that obtained for both $\varepsilon = 0$ and $\varepsilon = 1$. A considerable difference in the morphology of flow dynamics has been observed. In the lower layer, we note a rapid transient of the salt finger system from a regular array shape to an irregular shape. Indeed, the sinking fingers begin to interact quickly with each other resulting in a new reorganization of the finger structures.

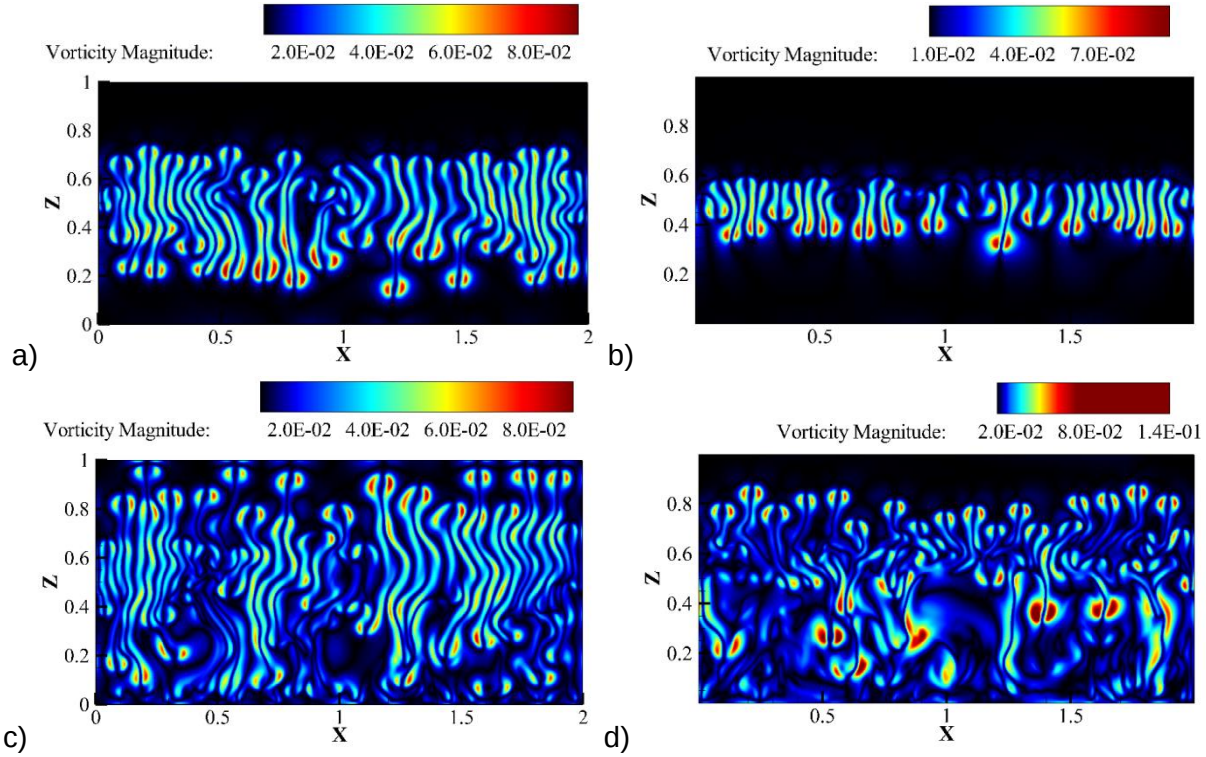

Figure 10. Instantaneous contours of vorticity modulus at moderate thermal Rayleigh number $Ra_T = 7.\times 10^6$ an $R_\rho = 6$: ($\varepsilon = 1$, left panel), ($\varepsilon = 3$, right panel).

As seen in figures 8 (d) and (f) the adjacent fingers approached each other and merged into finger-like plumes resulting hence a 'tree-like' with a branching pattern occupying a greater lateral space ranging $0 < Z < 0.2$ than at an early time. These plumes produce convective motions of strong recirculation cells (see, figure 8 (h)) making the system behavior dynamically and structurally much more complicated, figure 10 (d) depict this more clearly. The last phenomena play a prominent role in

the dynamic of mixing in the system as we will see later when inspecting the PDF fields.

Let us now look at the upper layer, one can observe the formation of small rising fingers (see figures 8 (d) and (f)), with a very small vertical velocity, kinetic energy and intense vorticity as shown in figures 9 (b) , (d) and 10 (b), hence, their vertical length cannot be extended and seem blocked due to the stable density stratification. More precisely, when sinking fingers reach the end rising fingers occup approximately 10% height of the computational domain as shown by figure 8 (f). This can be explained by a large diffusivity of the temperature field in the upper layer as shown in the figure 9 (f) where only arise wavy structures, and no thermal fingers can be detected. Conversely, in the same time, we observed the formation of mixed layer near the bottom boundary.

With time, the influence of the stabilizing temperature stratification diminished, and a rising fingers become able to accelerate again, hence, they commence to expand up progressively without interacting dynamically with each other even reaching the top boundary, conversely to the sinking ones. We also note that blobs are well-formed at the ends of the rising fingers. Figure 8 (j) also indicates that the nonlinear parameter affects the size of the rising fingers and leads to very thinner neck fingers.

Next, while the lower mixed layer continues to thicken upward into the mid-height of the computational domain, the upper mixed layer slowly builds up and takes place close to the top boundary. It is remarkable, then, that the asymmetric evolution of the dynamic of the flow system appears clearly in this case ($\varepsilon = 3$).

To deepen our insights about the influence of the nonlinear parameter on fingers the behavior, we calculate the average concentration of salinity in the horizontal direction for both cases $\varepsilon = 1$ and $\varepsilon = 3$. Figure 11 illustrates the horizontal averaged profils of

salinity at different times. At t=0 the initial distributions of the salinity take values $S^* = 0$ for $0 < Z < 0.5$ and $S^* = 1.0$ for $0.5 < Z < 1$ which corresponding to the salinity of the upper and lower layers respectively.

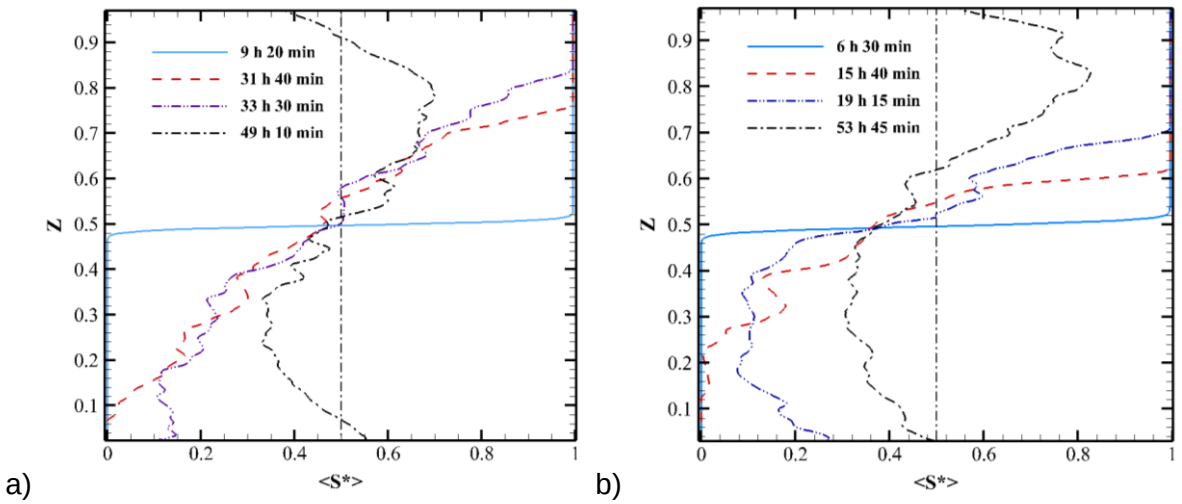

a) b)

Figure 11. Horizontally averaged mean of salinity profiles at moderate thermal Rayleigh number $Ra_T = 7.\times 10^6$ and $R_\rho = 6$: a) $\varepsilon = 1$, b) $\varepsilon = 3$.

It is interesting to note that initial salt profiles for both cases $\varepsilon = 1$ and $\varepsilon = 3$ at (t=9h 20 min) are almost identical to the initial distribution state with a weak change at the mid-height of the computational domain produced by diffusive processes. Obviously, in the diffusion phase, the symmetry of the profile is clearly remarkable, however, the break in symmetry is observed with the formation of fingers for (t>9 h 20 min). Indeed, salt profiles show clearly a dissimilarity in the spread zone distribution with respect to the mid-height owing to the difference in the velocity between rising and sinking fingers recall that the spread zone is the zone bounded between $<S^*>=0$ and $<S^*>=1$. This zone corresponds to the part of the computational domain invaded by the fingers. Because the system has asymmetric features, the spread zone can be redefined by two subzones, the first one is called the upper spread zone limited between $<S^*>=0.5$ and $<S^*>=1$, and the second one is called the lower spread zone limited between $<S^*>=0$ and $<S^*>=0.5$.

For $\varepsilon = 1$ (t = 31 h 40 min), the spreading zone in the upper layer extends from 0.5 to 0.7 i.e., $\Delta Z_{apper} = 0.25$, while in the lower layer, fingers reach the end of the bottom boundary which means that $\Delta Z_{lower} = 0.5$. Indeed, the growth rate between the two layers is $\Delta Z_{lower} / \Delta Z_{upper} = 2$. This discrepancy is due to the difference in the velocity between rising and sinking fingers.

For $\varepsilon = 3$ (t=15 h 40 min), the spreading zone in the upper layer extends from 0.5 to 0.6 i.e., $\Delta Z_{apper} \approx 0.1$, while in the lower layer $\Delta Z_{lower} = 0.5$. Indeed, the growth rate between the two layers is $\Delta Z_{lower} / \Delta Z_{upper} = 5$. This implies that increasing in asymmetric becomes more obvious when the nonlinear parameter increases. In addition, the sinking finger reach earlier the bottom layer for $\varepsilon = 3$ compared $\varepsilon = 1$. Moreover, the mixed zone develops early in the lower layer for both cases, where the salinity maintains its initial value $<S^*>=1$, which means that rising fingers have not yet reached the top of the boundary and continue to grow (t=33 h 30 min for $\varepsilon = 1$ and t=19 h 15 min for $\varepsilon = 3$). As time passes, we notice that the fluid continues to mix well near the bottom boundary which makes the profiles carried back quickly toward an asymptotic value of the salinity, around $<S^*>=0.5$. Moreover, the vertical gradient of the salinity ΔS^*_{lower} i.e., the salinity distribution is approximately equipartitioned and it becomes very weak with time leading to homogeneous mixing in the lower layer. We recall that $<S^*>=0.5$ is a good indicator of mixing efficiency. However, the upper mixed zone thickness is smaller than that of the lower and the profiles indicate clearly that the salinity value stays away from the asymptotic value $<S^*>=0.5$, conversely to the lower mixed zone. Additionally, the spread of the upper mixed zone toward the mid-height of the computational domain becomes slow when the nonlinear parameter is strong. This implies that the increase in the nonlinear

parameter diminishes the mixing intensity making the gradient of the salinity distribution in the vertical direction inhomogeneous. It is worth noting that the presence of fluctuations in the spreading zone is explained by the variation in the lengths of the fingers and their wavy shape.

To understand the nonlinear parameter on the mixing properties we now diagnose with scrutiny the temporal evolution of the probability density function (PDF) for salinity presented in figure 12.

Regardless of the first stage (not shown), we can clearly see that the increase of the nonlinear parameter affects significantly the mixing processes. A global glimpse of figure 12 reveals that there is an asymmetric in the salt mixing behavior compared to the linear case. The analysis of this figure exhibits a remarkable enhancement of mixing in the lower layer compared to the upper layer.

With the formation of the fingers, salt is transported vertically alternatively in upward and downward motions. The molecular diffusion between layers turns into horizontal diffusion through the sides surfaces that formed fingers.

For the weak nonlinear case $\varepsilon = 1$, figures 12 (a), (c), (e) and (g) show clearly that the mixing process evolution is not affected much by nonlinear parameter and seems much similar to those in the linear case (see the previous subsection) with a small delay in the mixing process between the upper and lower layers due to the faster growth of the sinking fingers, additionally, both rising and sinking evolve monotonically without interaction as in the linear case $\varepsilon = 0$.

However, for the high nonlinear case $\varepsilon = 3$, the mixing dynamics is completely different. Indeed, in figure 12 (b) in the lower layer, it is observed that the mixing process by molecular diffusion seems limited at $Z = 0.2$ in the upper layer because

the rising fingers grow slowly, while it remains diffuse rapidly in the lower layer as fingers continue to increase.

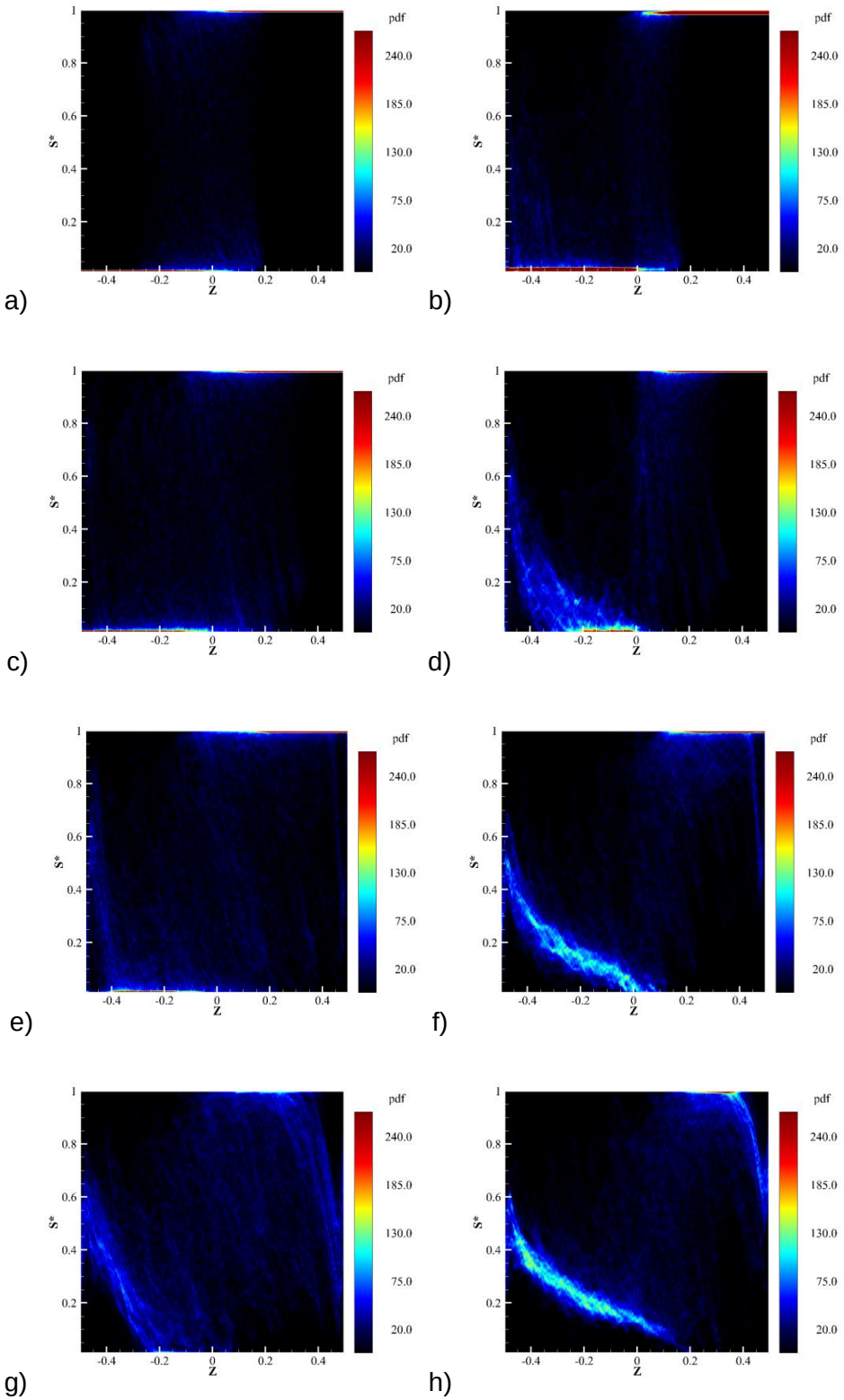

Figure 12. Evolution of the probability density function of the salinity at moderate thermal Rayleigh number $Ra_T = 7.\times 10^6$ and $R_\rho = 6$: ($\varepsilon = 1$left panel), ($\varepsilon = 3$,right panel).

One can also see the existence of a broad range where the salinity has values bounded between $0.6 < S^* < 0$ taking weak PDF values while zero pdf to find salinity values $0.6 < S^* < 1$. This dissimilarity in the PDF distribution implies that a small amount of salt ($S^* = 1$) that has been transported from the upper layer to the lower layer mixed earlier before reaching the bottom boundary due to the coalescence of salt finger structures with each other as shown figure 8 (f). The formation of tree-like strangles the sinking fingers and prevents then the transfer of salinity ($S^* = 1$) into the lower layer. Moreover, we also notice a high probability to find pure unmixed salt $S^* = 0$ in the system (figure 12 (b)) which indicates that the dynamic of mixing is very slow and dominates by diffusion process.

In figure 12 (d), mixing activity by convection becomes important in the region spanning $-0.5 < Z < -0.4$ where the most probable take values range between $0.4 < S^* < 0.6$ as shown by PDF distribution. This is directly related to the interaction of salt finger structures with the bottom boundary which leads to the formation of the lower mixed layer. Additionally, the probability of finding pure unmixed salinity ($S^* = 0$) stays high in the region spanning $-0.3 < Z < 0$ which implies that the no interaction of finger structures. In other words, the mixing by molecular diffusion is significant in this zone compared to the convective mixing. As time passes, the lower mixed layer thickens toward the mid-height of the computational ($Z = 0$), therefore,the probability to find a pure unmixed salinity ($S^* = 0$) is zero in this region, see figure 12 (f), meaning that the fluid in the lower layer is well-mixed.

On the other hand, in the upper layer, the PDF distribution in figure 12 (f) indicates that the mixing by molecular diffusion remains predominant and the diffusion zone continues to extend as the rising finger lengths increase. We also note the absence of salinity with values $S^* < 0.5$, and this can be explained straightforwardly by the fact

that the fingers become very thinner highly diffusive features which do not allow sufficiently the transport of fluid $S^* = 0$ from the lower to the upper layer. This finding is well corroborated by figure 8 (j). Moreover, the velocity of rising fingers is very weak, hence it takes time to reach the end of the computational domain and this promotes the diffusion mixing in this region. It must be noted that a high probability to find pure unmixed salt $S^* = 1$ is observed in the upper layer indicating that the mixing activity is very weak and is purely dominated by molecular diffusion.

In figure 12 (h), the high values of PDF for salinity values $S^* > 0.2$ take place in the lower layer which means that there is an intense mixing activity in this zone resulting from the vigorous convecting lower layer. This leads to the homogenization of the mixture in this zone. However, in the upper zone, close to the top boundary $Z > 0.4$, PDF ($S^* = 1$) is zero meaning that the rising fingers reach the top of the domain. However, it is also noted that the region $0.2 < Z < 0.4$ has high PDF values of salinity values $S^* = 1$ corresponding to the region in which the fingers have thinner neck structures. This means that mixing intensity is not sufficient to homogenize the distribution of salinity in this zone.

4. Conclusion

In this study, the impact of the density inversion, induced by the nonlinearity of the equation of state, on the development of the finger structures and their end state has been studied numerically. A high accuracy schemes have been employed to solve the two-dimensional Navier-Stokes equations with a nonlinear equation of state. The effects of nonlinear parameter have been investigated ($\varepsilon = 0$, $\varepsilon = 1$ and $\varepsilon = 3$) for high buoyancy ratio ($R_\rho = 6$) and moderate thermal Rayleigh number ($Ra_T = 7 \times 10^6$).

This paper forms a crucial key to understanding how density inversion modifies salt finger convection in cold regions, the main conclusions obtained are as follows: Compared with a linear equation of state we found that the nonlinear equation of state limits the vertical transport of the salt/heat and the kinetic energy, and depends on the nonlinear parameter values. The flow field analysis indicates that the increase of the nonlinear parameter affects the flow dynamics and the morphology of the salt fingers as well as the mixing process. In fact, the high nonlinear parameter modifies significantly the salt fingers evolution. The results show clearly the appearence of an asymmetric structure of the salt finger in the system and the finger pattern scenario is more complex at the lower layer where fingers develop quickly owing to the enhancement of the buoyancy force acting on them. Furthermore, in the low layer, the interaction between adjacent fingers is improved and the sinking fingers become disorderly in time. Conversely in the upper layer sinking fingers evolve slowly and monotonically without interacting with others. It should also be pointed out that the nonlinear parameter has no influence on the number of fingers developed in the system.

The effects of the density inversion on the mixing dynamics have also been discussed. The probability density function of the salinity PDF(S*) shows that at high nonlinear parameter mass transport and the mixing dynamics in the lower layer is enhanced while weakening in the upper layer with increasing in the nonlinear parameter. It also reveals that a weak nonlinear parameter has minor effect on the mixing process of the salinity.

In our future study, we will extend this work to reveal the influence of the density inversion on salt fingers convection for high and low thermal Rayleigh numbers and for different buoyancy ratios.

References

[1] R. W. Schmitt, Double diffusion in oceanography, Ann. Rev. Fluid Mech., 26, 255-285 (1985).

[2] J. Olsthoorn, E.W. Tedford, G. A. Lawrence, Salt-fingering in seasonally ice-covered lakes, Geophysical Research Letters, (2022).

[3] P. Garaud, A. Kumar, and J. Sridhar, The Interaction between Shear and Fingering (Thermohaline) Convection, The Astrophysical Journal, 879, Number 1 (2019).

[4] F. Suárez, S.W. Tyler, A.E. Childress, A fully coupled, transient double-diffusive convective model for salt-gradient solar ponds, Int. J. Heat Mass Transfer., 53, 1718-1730, (2010).

[5] A.C. Slim, M.M. Bandi, J.C. Miller, and L. Mahadevan, Dissolution-driven convection in a Hele-Shaw cell, Phys. Fluids, 25, 024101, (2013).

[6] C. F. Chen and J. S. Turner, Crystallization in a double-diffusive system, J. Geophys. Res. 85, 2573, (1980).

[7] R.W. Schmitt, The characteristics of salt fingers in variety of fluid systems, including stellar interiors, liquid metals, oceans, and magmas, Phys. Fluids, 26(9), 2373-2377 (1983).

[8] T. Bao, Z.L. Liu, Thermohaline stratification modeling in mine water via double-diffusive convection for geothermal energy recovery from flooded mines. Applied Energy, 237, 566-580, (2019).

[9] E. Hage and A. Tilgner, High Rayleigh number convection with double diffusive fingers.Phys.Fluids, 22, 076603-076607, (2010).

[10] R.W. Schmitt, Observational and laboratory insights into salt-finger convection, Prog. Oceanogr., 56, 419-433, (2003).

[11] A. Oschlies, H. Dietze, and P. Kahler, Salt-finger driven enhancement of upper ocean nutrient supply, Geophys. Res. Lett., 30, 2204, (2003).

[12] E. Kunze, Limits on growing, finite-length salt fingers: A Richardson number constraint,J. Mar. Res. 45, 533-556, (1987).

[13] R. W. Schmitt, Triangular and asymmetric salt fingers. Journal of Physical Oceanography, 24, 855-860 (1994).

[14] E. Kunze, A review of salt-fingering theory, Prog. Oceanogr. 56, 399-417, (2003).

[15] M. E. Stern, and T. Radko, The salt finger amplitude in unbounded T–S gradient layers. J. Mar. Res., 56,157-196, (1998).

[16] T.M. Özgökmen, O.E. Esenkov and D.B. Olson, A numerical study of layer formation due to fingers in double-diffusive convection in a vertically-bounded domain. J. Mar. Res., 56, 463-487, (1998).

[17] J. Yoshida, and H. Nagashima, Numerical experiments on salt-finger convection, Progress in Oceanography, 56 ,435-459, (2003).

[18] R. Krishnamurti, Double-diffusive transport in laboratory thermohaline staircases. J. Fluid Mech. 483, 287–314, (2003).

[19] J.Taylor, and G. Veronis, Experiments on double-diffusive sugar-salt fingers at high stability ratio, J. Fluid Mech., 321, 315-333, (1996).

[20] M. Kellner, and A. Tilgner, Transition to finger convection in double-diffusive convection. Phys. Fluids, 26, 094103 (2014).

[21] C.Y. Shen, and G. Veronis, Numerical simulation of two-dimensional salt fingers, J.Geophys. Res., 102, 23131-23143 (1997).

[22] K.R. Sreenivas, O.P. Singh and J. Srinivasan, On the relationship between finger width, velocity, and fluxes in thermohaline convection. Phys. Fluids, 21, 26601-26615, (2009).

[23] O.P. Singh and J. Srinivasan, Effect of Rayleigh numbers on the evolution of double-diffusive salt fingers. Phys. Fluids, 26, 062104-062118 (2014).

[24] R. Ouzani, Z. Alloui, Numerical study of two-dimensional salt-finger convection, Materials Today: Proceedings, 30, 833-837, (2020).

[25] R. Ouzani, Z. Alloui, S. Khelladi , and M. Specklin Dynamics of fingering convection: a numerical study, Environmental Fluid Mechanics, (2022).

[26] R. W. Schmitt, The growth rate of super-critical fingers, Deep-Sea Res. Oceanogr. Abstr. 26, 23-40, (1979).

[27] S. A. Piacsek and J. Toomre, Nonlinear evolution and structure of salt fingers, in Marine Turbulence, Elsevier Oceanography Series, 28, 193-219, (1980).

[28] J. Olsthoorn, E. W. Tedford and G. A. Lawrence, The cooling box problem: convection with a quadratic equation of state, J. Fluid Mech. 918 (2021).

[29] J. Olsthoorn, E. W. Tedford, G. A. Lawrence, Salt-fingering in seasonally ice-covered lakes. Geophysical Research Letters, 49 (2022).

[30] T. M. Özgökmen, and O. E. Esenkov, Asymmetric salt fingers induced by a nonlinear equation of state, Physics of Fluids, 10, 1882, (1998).

[31] T. J. McDougall, Double-diffusive convection with a non-linear equation of state. Part II. Laboratory experiments and their interpretation, Prog. Oceanogr. 10, 91, (1981).

[32] R. W. Schmitt, Flux measurements at an interface, J. Mar. Res. 37, 419, (1979).

[33] J. Olsthoorn, E. W. Tedford and G. A. Lawrence, The cooling box problem: convection with a quadratic equation of state, J. Fluid Mech. 918, A6, (2021).

[34] L. A. Couston, D. Lecoanet, B. Favier, and M. Le bars, Order out of chaos: slowly reversing mean flows emerge from turbulently generated internal waves. Phys. Rev. Lett. 120, 244505, (2018).

[35] S. Toppaladoddi, and J. S. Wettlaufer, Penetrative convection at high Rayleigh numbers, Phys. Rev. Fluid, 3, 043501, (2018).

[36] Y. Yang, W.Y. Chen, R. Verzicco, and D. Lohse, Multiple states and transport properties of doublediffusive convection turbulence. Proc. Natl. Acad. Sci. U.S.A. 117 , 14676-14681, (2020).

[37] C.Y. Shen, Heat-salt finger fluxes across a density interface, Phys. Fluids, 5, 2633-2643, (1993).

[38] K. Kamakura and H. Ozoe, Numerical analysis of salt-finger phenomena near the interface between two liquid layers in a cubic enclosure, Numer. Heat Transfer, Part A, 40, 861, (2001).

[39] J. Li, and Y. Yang, On the wall-bounded model of fingering double diffusive convection, , (2022). https://doi.org/10.48550/arXiv.2204.03142

[40] A. Traxler, S. Stellmach, P. Garaud, T. Radko, and N. Brummell, Dynamics of fingering convection. Part 1 Small-scale fluxes and large-scale instabilities. J. Fluid Mech. 677, 530-553, (2011).

[41] F. Oueslati, B. Ben-Beya, T. Lili, Double-diffusive natural convection and entropy generation in an enclosure of aspect ratio 4 with partial vertical heating and salting sources, Alex. Eng. J. 52, 605-625, (2013)

[42] C.W. Shu, High order ENO and WENO schemes for computational fluid dynamics, in High-Order Methods for Computational Physics, T.J. Barth and H. Deconinck, editors, Lecture Notes in Computational Science and Engineering, Springer, 9, 439-582, (1999).

[43] C.W. Shu, Essentially non-oscillatory and weighted essentially non-oscillatory schemes for hyperbolic conservation laws, in Advanced Numerical Approximation of

Nonlinear Hyperbolic Equations, Lecture Notes in Math. 1697, Springer-Verlag, Berlin, 325-432, (1998).

[44] S. Gottlieb, C.W. Shu, Total variation diminishing Runge–Kutta schemes, Math.Comput., 67,73-85, (1998).

[45] T. Nishimura, M. Wakamatsu, A.M. Morega, Oscillatory double diffusive convection in a rectangular enclosure with combined horizontal temperature and concentration gradients, Int J Heat Mass Transfer., 41(11), 1601-1611, (1998).

[46] Q. Qin, Z.A. Xia, Zhen F. Tian. High accuracy numerical investigation of double-diffusive convection in a rectangular enclosure with horizontal temperature and concentration gradients, Int. J. Heat Mass Transfer, **71**, 405–423, (2014).

[47] A. J. Chamkh, H. Al-Naser Hydromagnetic double-diffusive convection in a rectangular enclosure with opposing temperature and concentration gradients, Int. J. Heat Mass Transfer, **45,** 2465-2483, (2002).

[48] A.A.A.A. Al-Rashed, H.F. Oztop, L. Kolsi, A. Boudjemline, M. A. Almeshaal, M. E. Ali, Ali Chamkha. CFD study of heat and mass transfer and entropy generation in a 3D solar distiller heated by an internal column. Int. J. Mech. Sci. **152**, 280-288 (2019).

[49] Y. Yang, E. P. van der Poel, R. Ostilla-Mónico, C. Sun, R. Verzicco, S. Grossmann and D. Lohse, Salinity transfer in bounded double diffusive convection, J. Fluid Mech., 768 , 476- 491, (2015).

[50] Y. Yang, R. Verzicco, and D. Lohse, Scaling laws and flow structures of double diffusive convection in the finger regime. J. Fluid Mech. 802, 667-689, (2016).

[51] J.R.Taylor, and G. Veronis, Experiments on salt fingers in a Hele Shaw cell, Science, 231, 39-41, (1986).

[52] S.E. Pringle, and R.J. Glass, Double-diffusive finger convection: influence of concentration at fixed buoyancy ratio. J. Fluid Mech., 462, 161-183, (2002).

[53] F. Rehman and O.P. Singh, Salt finger convection at marginal stability, Geo & Astro Fluid dynamics, 11(5),323-332, (2017).

[54] S.A. Stanley, S. Sarkar and J.P. Mellado. A study of the flow-field evolution and the mixing in a plane turbulent jet using direct numerical simulation. J. Fluid Mech. 450, 377-407, (2002).

[55] P.S. Karasso, and M.G. Mungal. Scalar mixing and reaction in plane liquid shear layers. J. Fluid Mech. **323**, 23-63, (1996).

[56] M. Rogers, and M. Moser, R. D. Direct simulation of a self-similar turbulent mixing layer Phys. Fluids, **6**, 903-923, (1994).